Three-Species Collisionless Reconnection: Effect of O^+ on Magnetotail Reconnection

M. A. Shay* and M. Swisdak

Institute for Research in Electronics and Applied Physics, University of Maryland, College Park, Maryland, 20742, USA

The nature of collisionless reconnection in a three-species plasma composed of a heavy species, protons, and electrons is examined. In addition to the usual two length scales present in two-species reconnection, there are two additional larger length scales in the system: one associated with a "heavy whistler" which produces a large scale quadrupolar out-of-plane magnetic field, and one associated with the "heavy Alfvén" wave which can slow the outflow speed and thus the reconnection rate. The consequences for reconnection with O^+ present in the magnetotail are discussed.

Introduction.—Recent studies of collisionless reconnection have shown that the disparate masses of the ions and electrons lead to a two-scale dissipation region near the x line. The decoupling of the ions from the magnetic field at larger scales than the electrons can lead to whistler or kinetic Alfvén physics in the dissipation region, whose quadratic dispersive characteristics can substantially increase the reconnection rate [1–4]. A Sweet-Parker-like [5] analysis of this dissipation region yields insight into the reconnection rate: $V_{in} \sim (\delta/D)c_{At}$, where V_{in} is the inflow speed, δ and D are the width and length of the dissipation region, and c_{At} is the Alfvén speed just upstream from the dissipation region.

Many plasma systems have heavier species, in addition to protons and electrons, which may play an important dynamical role: negatively charged dust grains in astrophysical molecular clouds and the interstellar medium, and O^+ in the Earth's magnetosphere [6]. Previous simulations of three-species reconnection have focused on O^+ in the magnetosphere [7–9], where the number density of O^+ can sometimes exceed that of the protons [10,11]. These simulations, however, either did not find any effect of O^+ on reconnection due to the small system size or did not spatially resolve the reconnection boundary layers.

In this Letter we present the first comprehensive study of basic three-fluid reconnection showing through theory and simulation both the effect of the heavy species on the reconnection rate and the hierarchy of scales present in the microscale boundary layers. We find that the usual two scales associated with collisionless two-fluid reconnection ($d_i = c/\omega_{pi}$, $d_e = c/\omega_{pe}$) are instead replaced by four scales. The inner two scales are associated with a light whistler and a light Alfvén wave, which are very similar to their two-fluid counterparts. At larger scales, however, a heavy whistler and heavy Alfvén wave occur. The heavy whistler can occur on scales much larger than a d_i and thus gives rise to a much wider quadrupolar out-of-plane magnetic field signature. Associated with this magnetic field are parallel ion Hall currents, the analogue to the light whistler electron currents. The higher O^+ mass substantially slows the reconnection rate because

the outflow speed from the x line is reduced from the usual proton Alfvén speed, c_{Ai}, to the much slower heavy Alfvén speed, c_{At}.

Analytical Analysis.—We begin with the general three-fluid equations [12] and first ignore electron inertia so that $\mathbf{E} = -\mathbf{V}_e/c \times \mathbf{B} - \nabla P_e/(n_e e)$. We assume quasineutrality, $n_e = n_i + z_h n_h$, where n_i is the light ion density, n_h is the heavy species density, and z_h is the charge number of the heavy species. We ignore the displacement current, $\mathbf{J} = (c/4\pi)\nabla \times \mathbf{B}$. We normalize length to $d_i = c\sqrt{m_i}/\sqrt{4\pi n_{i0}e^2}$ and time to $\Omega_i^{-1} = m_i c/(eB_0)$, which gives the following equations:

$$\frac{\partial n_\alpha}{\partial t} = -\nabla \cdot (n_\alpha \mathbf{V}_\alpha), \quad \alpha = \{i, h\}, \quad (1)$$

$$n_i \frac{d\mathbf{V}_i}{dt} = z_h n_h (\mathbf{V}_e - \mathbf{V}_h) \times \mathbf{B} + \mathbf{J} \times \mathbf{B} - \nabla P_i - \frac{n_i}{n_e}\nabla P_e, \quad (2)$$

$$\hat{m}_h n_h \frac{d\mathbf{V}_h}{dt} = z_h n_h (\mathbf{V}_h - \mathbf{V}_e) \times \mathbf{B} - \nabla P_h - \frac{z_h n_h}{n_e}\nabla P_e, \quad (3)$$

$$\frac{\partial \mathbf{B}}{\partial t} = \nabla \times (\mathbf{V}_e \times \mathbf{B}), \quad (4)$$

where $n_e \mathbf{V}_e = n_i \mathbf{V}_i + z_h n_h \mathbf{V}_h - \mathbf{J}$, $d\mathbf{V}_\alpha/dt = (\partial/\partial t + \mathbf{V}_\alpha \cdot \nabla)\mathbf{V}_\alpha$, $\hat{m}_h = m_h/m_i$, $\mathbf{J} = \nabla \times \mathbf{B}$, and $P_\alpha = T_\alpha n_\alpha$, where T_α is assumed to be an unchanging spatial constant (isothermal approximation).

Although reconnection is a highly nonlinear process, much information about its nature can be gleaned from a linear analysis, for it is bent field line waves which ultimately accelerate the plasma away from the x line. We write each variable as $\mathbf{f}(\mathbf{x}, t) = \mathbf{f}_0(\mathbf{x}) + \tilde{\mathbf{f}}e^{i(\mathbf{k}\cdot\mathbf{x} - \omega t)}$. Beginning with a uniform $\mathbf{B}_0$ with no initial velocities, we proceed to linearize Eqs. (1)–(4) and assume that $\mathbf{k} \parallel \mathbf{B}_0$ for simplicity. The sound waves with $\mathbf{k} \parallel (\mathbf{V}_i$ and $\mathbf{V}_h)$ decouple from the magnetic waves, leaving the following dispersion relation:

$$\frac{\omega^3}{\Omega_i^3} \pm \frac{\omega^2}{\Omega_i^2}\left[\frac{z_h n_h}{n_e} - \frac{\Omega_h}{\Omega_i}\frac{z_h n_h}{n_e} + \frac{\Omega_h}{\Omega_i} - k^2 d_s^2\right] -$$

$$\frac{\omega}{\Omega_i} k^2 d_s^2\left[1 + \frac{\Omega_h}{\Omega_i}\right] \mp k^2 d_s^2 \frac{\Omega_h}{\Omega_i} = 0, \quad (5)$$

where $\Omega_i = eB_0/(m_i c)$, $\Omega_h = ez_h B_0/(m_h c)$, $d_s = d_i\sqrt{n_i/n_e} = c\sqrt{m_i}/\sqrt{4\pi n_e e^2}$, $d_h = c\sqrt{m_h}/\sqrt{4\pi n_h z_h^2 e^2}$, $n_e = n_i + z_h n_h$, and all densities n are equilibrium quantities. This equation is fully general and can apply to any plasma with electrons, ions, and a third species.

Balancing the second and fourth terms and taking the limit $\omega \ll \Omega_h \lesssim \Omega_i$ and $k^2 d_h^2 \ll 1$ yields the largest scale or global Alfvén wave: $\omega = \pm kc_{At}$, where $c_{At} = B/\sqrt{4\pi(m_h n_h + m_i n_i)}$. In order for the heavy species to slow the global Alfvén wave appreciably, it is necessary for $m_h n_h \gg m_i n_i$.

Taking the limit of $\Omega_i \gg \Omega_h$, $\omega \gg \Omega_h$, and $m_h n_h \gg m_i n_i$ yields the high frequency dispersion

$$\frac{\omega^2}{\Omega_i^2} \pm \frac{\omega}{\Omega_i}\left(\frac{z_h n_h}{n_e} - k^2 d_s^2\right) - k^2 d_s^2 = 0. \quad (6)$$

For $|z_h|n_h/n_e \lesssim 1$, this equation produces the light whistler, the light Alfvén, and the heavy whistler waves shown in Fig. 1, where $d_h^2 = c^2 m_h/(4\pi n_h z_h^2 e^2)$ and $c_{Ah} = B/\sqrt{4\pi n_h m_h}$. The existence of the heavy whistler wave has been noted in electron-positron-dusty plasmas [13] and electron-proton-dusty plasmas [14,15], but was not applied to reconnection. Taking $k^2 d_s^2 n_e/|z_h n_h| \gg 1$, and then equating the first and second terms yields the light whistler with $\omega = \pm k^2 d_i c_{Ai}(n_i/n_e)$, where $c_{Ai} = B/\sqrt{4\pi m_i n_i}$ is the proton Alfvén speed. Equating the first and third term yields the light Alfvén wave with $\omega = \pm kc_{Ai}\sqrt{n_i/n_e}$. The transition between these two waves occurs when $k^2 d_s^2 \sim 1$. Both of these waves are very similar to their two-species analogues except n_i has been replaced with n_e.

Taking $k^2 d_s^2 n_e/|z_h n_h| \ll 1$ and equating the first and third terms also yields the light Alfvén wave. Equating the second and third term yields the heavy whistler wave with $\omega = \pm k^2 d_h c_{Ah}$. The transition between these two waves occurs at $k^2 d_i^2 n_i n_e/(z_h^2 n_h^2) \sim 1$. The heavy whistler
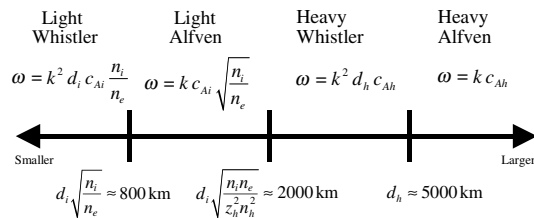

FIG. 1. (below line) The nonideal length scales present in three-fluid reconnection and numbers for typical magnetotail lobes with O^+ present [10] ($n_i = 0.05$ cm^{-3}, $n_h/n_i = 0.64$). (above line) Waves and dispersion relations at each scale range.

requires $\omega \gg \Omega_h$ so that the heavy species is unmoving, but the ion inertia term in Eq. (2) is negligible. Thus, the wave is characterized by frozen-in protons and electrons that flow together and act as a massless fluid, but because $n_i \neq n_e$, this net flow is a current. This wave transitions to the heavy Alfvén wave at $kd_h \sim 1$ with $\omega = kc_{Ah}$ in this limit.

The two-scale structure of the dissipation region in a collisionless two-fluid plasma [16] (d_e and d_i) has now been replaced with four scales: the three scales in Fig. 1 plus a very small electron scale δ_e where the electron frozen-in constraint is broken. We did not include δ_e in this calculation to simplify the analysis and because δ_e does not appear to substantially modify the reconnection rate in well developed Hall mediated reconnection [17].

Simulations.—Equations (1)–(4) with $z_h = 1$ and the same normalizations were integrated forward in time using F3D, a parallel fluid code. The simulation domain is a uniform grid of 2048×1024 grid points with the physical size $L_x \times L_z = 204.8 \times 102.4$, with periodic boundaries at $x = \pm L_x/2$ and $z = \pm L_z/2$. The initial equilibrium consists of a system size double current sheet with $B_x = B_0\{\tanh[(z + L_z/4)/w_0] - \tanh[(z - L_z/4)/w_0] - 1\}$ and $w_0 = 1.5$. $\mathbf{V}_h = 0$ initially with $n_h = 0.64$ everywhere and $T_i = T_e = T_h = 0.5$. Pressure balance is maintained by setting $B^2/2 + (T_i + T_e)n_i = B_0^2/2 + (T_i + T_e)n_{i0}$, where $B_0 = 1.0$ and $n_{i0} = 1.0$ are the values outside the current sheet. A final equilibrium constraint is $n_i V_{iy} = J_y T_i/(T_i + T_e)$, which determines V_{iy}. The remainder of the equilibrium current is put into V_{ey}. In order to break the frozen-in constraint of the electrons at the smallest scales, the term $\mu_4 \nabla^4 \mathbf{B}$ has been added to the right-hand side of Eq. (4), with $\mu_4 = 5 \times 10^{-5}$. To initialize the double tearing mode, x lines were seeded in both current sheets at $(x, z) = (\pm L_x/4, \mp L_z/4)$ with an initial half island width $w = 0.55$. A small amount of random noise was added to the initial $\mathbf{B}$ and $\mathbf{V}_i$ of about 10^{-3} their equilibrium values.

To examine the effect of the heavy ion mass, We ran three simulations with $\hat{m} = \{1, 16, 10^4\}$ and $n_h = 0.64$ in all cases. The first case corresponds to the usual two-species reconnection. The second case corresponds to reconnection in the presence of O^+, with $\{d_s, d_i\sqrt{n_i n_e/(z_h n_h)^2}, d_h\} = \{0.8, 2, 5\}$. In the third case, the 3 length scales are $\{0.8, 2, 125\}$, so that the heavy ions form an immovable background and the global scales are controlled by the heavy whistler.

The reconnection rates of the three simulations versus time are shown in Fig. 2(a). The $\hat{m}_h = 1$ case clearly shows a substantially larger reconnection rate. The two cases with heavy ions show very similar reconnection rates, but the largest $\hat{m}_h$ shows a large decrease in its reconnection rate around $t = 600$, while the $\hat{m}_h = 16$ case keeps a steady rate. The heavy whistler velocity has a k dependence, $V \sim kd_h c_{Ah}$. As reconnection proceeds in a system and the island width w gets larger and
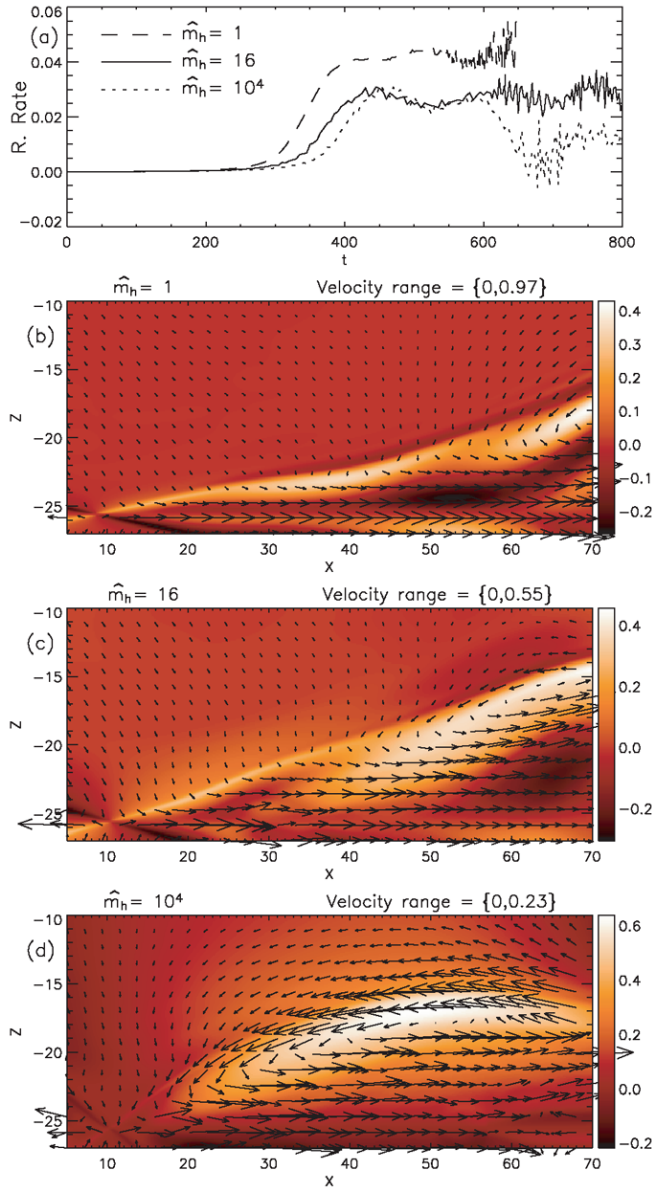
FIG. 2 (color online).   (a) Reconnection rates. (b)–(d) B_y with proton flows, (b) $\hat{m}_h = 1$ and $t = 500$, (c) $\hat{m}_h = 16$ and $t = 650$, (d) $\hat{m}_h = 10^4$ and $t = 650$.

larger, the effective $k \sim 1/w$ for the reconnection process decreases. Because the heavy whistler is mediating global convection in the $\hat{m}_h = 10^4$ case, as the global convection scale length increases, the global convection velocity must decrease, throttling the reconnection rate.

The reconnection generates very different signatures for the different $\hat{m}_h$. Figs. 2(b)–2(d) show the out-of-plane B_y generated from the reconnection and the proton flow vectors. The x line is located close to $(x, z) = (10, -25.6)$ in all three cases. Only a small fraction of the total simulation is shown. The $\hat{m}_h = 1$ case shows the usual quadrupolar structure generated by frozen-in electron flow [18]. For $x > 45$, the clean quadrupolar signature begins to change to a more complicated structure

with both positive and negative B_y due to the finite system size. Because V_{ix} is maximum at about $x = 45$, and for greater x the slow-down of V_{ix} causes a compression of B_z, and the resulting J_y generates a B_y signature of the opposite sign.

The $\hat{m}_h = 16$ case [Fig. 2(c)] shows signatures of both the light and heavy whistler. For $x < 40$ a narrow band of positive B_y associated with the light whistler is present. A cut of B_y, V_{ix}, and V_{hx} at $x = 20$ is shown in Fig. 3. This B_y spike has a main length scale of about a d_i, which is roughly consistent with the light whistler cutoff scale of $d_s = 0.8$ for this simulation. Like the usual two-species whistler, the in-plane current generating this B_y is due to counterstreaming parallel electron beams upstream and downstream of the B_y perturbation. There is a long tail of B_y upstream of the spike ($z > -23.5$) in Fig. 3(a), though, which is not present in the two-species case. The proton outflow shows a peak on the symmetry axis like the two-fluid case, and its velocity is much larger than the O$^+$ velocity.

The quadrupolar B_y becomes dominated by the heavy whistler for $x > 40$ in the $\hat{m}_h = 16$ case. The B_y signature broadens out substantially because $d_h = 5$ for this simulation, and the current which generates it is carried by both the ions and electrons. Figure 4(a) shows comparison slices for the $\hat{m}_h = 1$ and 16 cases at $x = 55.0$. The main positive B_y spike is substantially wider in the $\hat{m}_h = 16$ case, although it is not 5 times wider as might be expected from a comparison of d_h to d_i. The x velocities reveal another key signature, as shown in Fig. 4(b) for $\hat{m}_h = 16$. The parallel ion flows from the heavy whistler associated with B_y lead to a negative V_{ix} at about $z = -17$. Also, the ion flow no longer is maximum at the symmetry line, but instead peaks off axis at around $z = -20.5$. On the symmetry line, V_{hx} is somewhat larger than V_{ix}. V_{ix} is about 4 times slower in the $\hat{m}_h = 16$ case than in the $\hat{m}_h = 1$ case. The off axis peak of V_{ix} and the substantial negative V_{ix} (about $1/3$ of maximum ion outflow) do not occur unless the heavy whistler is active.

In the case with $\hat{m}_h = 10^4$, the heavy ions are immovable and the heavy whistler is dominant at the global scales in the simulation as seen in Fig. 2(d). The main peak of B_y is quite wide, and there is a nonzero B_y out to
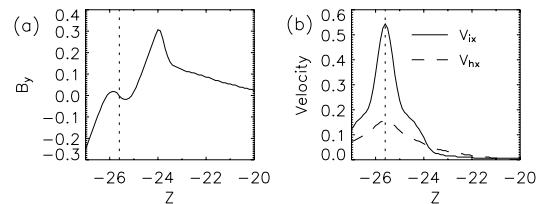

FIG. 3.   For the O$^+$ case, a cut along z at $x = 20.0$: (a) B_y and (b) V_{ix} and V_{hx}. The vertical dotted line is the symmetry axis ($z = -25.6$).
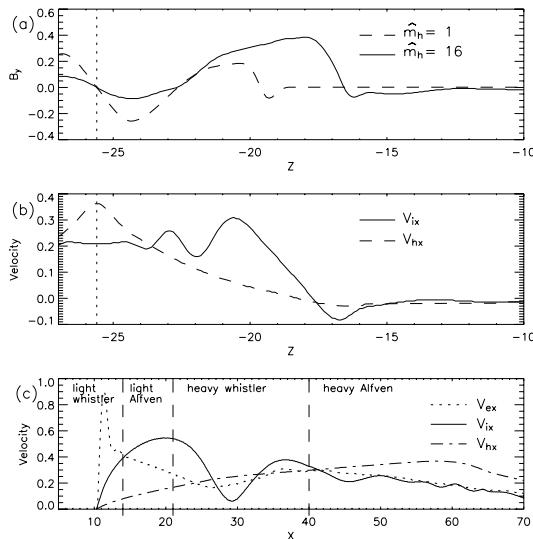
FIG. 4. (a) Slice of B_y along z at $x = 55$, (b) slice of x velocities along z at $x = 55$ for $\hat{m}_h = 16$, (c) slice of x velocities along x at $z = -25.6$ for $\hat{m}_h = 16$.

global scales. The parallel ion flows which flow with the Hall electron currents are much stronger in this case.

The multiscale structure of the dissipation region is demonstrated for the O^+ case in a cut of the outflows away from the x line, as shown in Fig. 4(c), which is a cut along x through the center of the current sheet. For $x < 21$, the behavior of the flows is very similar to that seen in two-species reconnection [4,19]. In the light whistler region, the electrons accelerate to speeds much faster than the ions and exceeding the relevant Alfvén speed. The electrons cannot maintain this high velocity and are forced to decelerate to a speed comparable to the protons when they reach the light Alfvén region. Inside of this Alfvén region, the protons reach their maximum velocity. The protons, in an analogy to the electrons in the light whistler region, cannot flow this speed indefinitely, and are forced to slow down inside the heavy whistler region. Finally, their speed becomes comparable to the O^+ outflow in the heavy Alfvén region. Inside the heavy whistler region at $x = 29$, however, V_{ix} drops nearly to zero, below V_{hx}. This behavior also occurs in the $\hat{m}_h = 10^4$ case at about $x = 18$, as seen in Fig. 2(d). The O^+ outflows behave like the proton outflows in the two-fluid case, gradually accelerating and finally reaching their maximum velocity in the outermost Alfvén region.

Discussion.—As discussed in the introduction, a Sweet-Parker—like analysis of the dissipation region yields $V_{in} \sim (\delta/D)c_{At}$. For the $\hat{m}_h = \{1, 16\}$ cases, we would expect the outflow speeds to differ by a factor of $\sqrt{(m_i n_{i16} + m_h n_h)/(n_{i1} m_i)} = 2.6$ between the two cases, where $n_{i1} = 1.64$, $n_{i16} = 1.0$, and $n_h = 0.64$. The maximum outflow in the two-species case is about 1.0, while for the case with O^+ is 0.35, giving a ratio of 2.9, quite close to what is expected. If δ/D stayed the same between

the two simulations, the O^+ case would be expected to reconnect nearly 3 times slower than the two-species case. In Fig. 2(a), however, the two cases asymptote to approximately steady-state rates that differ by around 1.5, leaving a factor of about 2 unaccounted for. A rough estimation of the scaling of δ/D between the simulations may be possible by examining the angle θ that the B_y signature makes with the $z = -25.6$ symmetry line. Presumably $\delta/D \sim \tan\theta$. This gives $\tan\theta_1 = 0.08$ and $\tan\theta_{16} = 0.15$, which sheds light on the factor of 2 difference. A more careful determination of δ/D as well as a scaling study with very large system sizes will be necessary to determine if this change in δ/D is robust.

These results imply that a substorm occurring with a high enough O^+ density ($m_h n_h \gg m_i n_i$) will have slower outflows and a reduced reconnection rate normalized to the upstream proton Alfvén speed. With all else being equal, this implies that the expansion phase of substorms will take longer to occur or will reconnect less lobe field in the same amount of time. However, substantial O^+ populations tend to occur during times of increased geomagnetic activity. The magnetotail equilibrium, and thus the lobe magnetic fields and density, may be modified substantially during these periods, which may offset or even overpower the reduction in the reconnection rate.

   *Email address: shay@glue.umd.edu
   Electronic address: http://www.glue.umd.edu/~shay
[1] J. Birn *et al.*, J. Geophys. Res. **106**, 3715 (2001).
[2] D. Biskamp *et al.*, Phys. Rev. Lett. **75**, 3850 (1995).
[3] B. N. Rogers *et al.*, Phys. Rev. Lett. **87**, 195004 (2001).
[4] M. A. Shay *et al.*, Geophys. Res. Lett. **26**, 2163 (1999).
[5] V. M. Vasyliunas, Rev. Geophys. **13**, 303 (1975) .
[6] E. G. Shelley *et al.*, J. Geophys. Res. **77**, 6104 (1972).
[7] J. Birn *et al.*, Ann. Geophys. **22**, 1305 (2004).
[8] M. Hesse and J. Birn, Ann. Geophys. **22**, 603 (2004).
[9] R. M. Winglee, J. Geophys. Res. **109**, A09206 (2004).
[10] L. M. Kistler *et al.*, J. Geophys. Res. (to be published).
[11] W. K. Peterson *et al.*, J. Geophys. Res. **86**, 761 (1981).
[12] J. Harold and A. B. Hassam, J. Geophys. Res. **99**, 19 325 (1994).
[13] P. K. Shukla *et al.*, Astron. Astrophys. **317**, L21 (1997).
[14] G. Ganguli and L. Rudakov, Phys. Rev. Lett. **93**, 135001 (2004).
[15] L. I. Rudakov, Phys. Scr. **T89**, 158 (2001).
[16] M. A. Shay *et al.*, J. Geophys. Res. **25**, 9165 (1998).
[17] M. A. Shay and J. F. Drake, Geophys. Res. Lett. **25**, 3759 (1998).
[18] M. E. Mandt *et al.*, Geophys. Res. Lett. **21**, 73 (1994).
[19] M. A. Shay *et al.*, Phys. Plasmas **11**, 2199 (2004).